John von Neumann Institute for Computing

Molecular Dynamics Computer Simulation of Multicomponent Liquids: From Effective Potentials to Crystallization from the Melt

A. Kerrache, A. Carré, J. Horbach, K. Binder

published in

NIC Symposium 2008,
G. Münster, D. Wolf, M. Kremer (Editors),
John von Neumann Institute for Computing, Jülich,
NIC Series, Vol. **39**, ISBN 978-3-9810843-5-1, pp. 205-212, 2008.

http://www.fz-juelich.de/nic-series/volume39

Molecular Dynamics Computer Simulation of Multicomponent Liquids: From Effective Potentials to Crystallization from the Melt

Ali Kerrache[1], Antoine Carré [1], Jürgen Horbach[1,2], and Kurt Binder[1]

[1] Institut für Physik, Johannes-Gutenberg-Universität Mainz
Staudinger Weg 7, 55099 Mainz, Germany
E-mail: kurt.binder@uni-mainz.de

[2] Institut für Materialphysik im Weltraum, Deutsches Zentrum für Luft- und Raumfahrt (DLR)
51170 Köln, Germany
E-mail: juergen.horbach@dlr.de

The molecular dynamics (MD) simulation technique is a powerful tool for the investigation of multicomponent liquids and solids. A realistic description of such systems relies on the quality of the effective potential with which the interactions between the atoms are modelled in a MD simulation. We propose a fitting scheme to derive effective potentials from *ab initio* simulations. This scheme is used to parametrize a new potential for silica. In a second case study, MD simulations are used to investigate crystallization in an AlNi alloy, elucidating the crystal growth mechanism on an atomistic scale.

1 Introduction

Molecular dynamics (MD) computer simulations describe the structure and dynamics of condensed matter systems on an atomistic scale[1–4]. In a MD simulation, Newton's equations of motion are solved numerically for an interacting many particle system. As a result, one obtains the trajectories of the particles from which one can calculate, in principle, any static or dynamic quantity of interest. This allows to shed light, e.g., on microscopic transport processes in binary (glassforming) liquids[5].

But how realistic can one model a multicomponent liquid by MD simulation? This depends on the quality of the effective potential that is used to model the interactions between the atoms. To obtain such a potential model for a given system, one usually fits the parameters of some given functional form of the potential to *ab initio* calculations or to experimental data. Very recently, we have proposed a fitting scheme to obtain an effective potential from an *ab initio* MD simulation technique, the so-called Car-Parrinello molecular dynamics (CPMD)[7]. We have used this scheme to parameterize a new pair potential for amorphous silica (SiO_2)[6]. In Sec. 2, we show that our new potential provides an accurate description of the tetrahedral network structure as well as the diffusion dynamics of SiO_2.

With a reliable model potential, one can get insight into microscopic transport mechanisms of real materials. An old problem is to clarify the mechanism of crystal growth from the melt (see, e.g., Ref.[8,9]). In Sec. 3, we consider the crystal growth kinetics of the binary alloy $Al_{50}Ni_{50}$. The experimental melting temperature for this system is at 1920 K where it exhibits a first order phase transition from a liquid to an intermetallic B2 phase. Recent experiments have shown that the crystal growth velocity for this transition is relatively slow[10]. At an undercooling of about 60 K, growth velocities of the order of 0.1 m/s were found. This value is about two orders of magnitude smaller than that found for pure

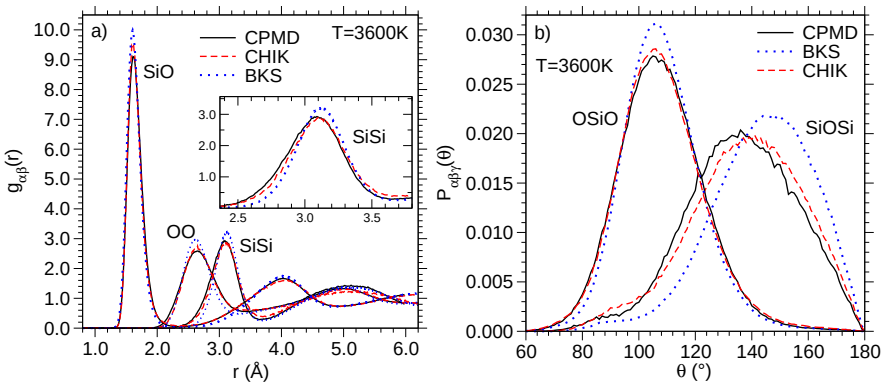

Figure 1. a) Partial pair correlation functions at $T = 3600\,\mathrm{K}$ for the SiSi, SiO, and OO correlations, calculated from CPMD and classical MD using the BKS and the CHIK potentials, as indicated. The inset shows an enlargement of the first peak in $g_{\mathrm{SiSi}}(r)$. b) Angular distribution functions for the OSiO and SiOSi angle at $T = 3600\,\mathrm{K}$, as obtained from CPMD and classical MD with the BKS and the CHIK potential.

metals at comparable undercoolings. The MD simulation sheds light onto the nature of the slow crystal growth in $Al_{50}Ni_{50}$, indicating that diffusion processes in the liquid-crystal interface control the speed of the growth kinetics[11].

2 A New Effective Potential for Silica

In a CPMD simulation, the electronic degrees of freedom are explicitly taken into account on a quantum mechanical level in the framework of density functional theory[12]. Nowadays, systems of 100 to 200 particles can be simulated on a time scale of several tens of picoseconds by CPMD. Apart from studying the structural and dynamic properties of a material, one can also use this technique to derive effective potentials for classical MD simulations, the latter technique providing simulations on much larger scales than CPMD. To obtain an effective potential for a given system, one first has to decide about its functional form. A pair potential model, the so-called BKS potential[13], has been shown to give quite an accurate description of amorphous silica, though it has some deficiencies (e.g., the density of amorphous silica is not well reproduced). In this work, we aimed at developing a pair potential model that is better than the BKS model, in particular with respect to the density. The second step in the development of the potential is to fit the free parameters to the CPMD calculations. This is a non-trivial task since one has to match the CPMD trajectories to a high-dimensional fit parameter space. To this end, we have developed a new iterative fitting scheme that is based on the matching of the partial pair correlation functions from MD runs of the effective potential model with those from CPMD runs. The details of the MD simulations and of the fitting scheme can be found in Refs.[6,14]. As a result, we obtained a new pair potential for silica that we call CHIK potential.

In the following, we compare structural and dynamic quantities, as calculated by CPMD and classical MD, using the BKS and the CHIK model.

Figure 1a shows the partial pair correlation functions[5] at $T = 3600\,\mathrm{K}$, as calculated from CPMD and classical MD using the BKS and the CHIK potential, as indicated. The CHIK model yields good agreement with the CPMD results. The largest differences are

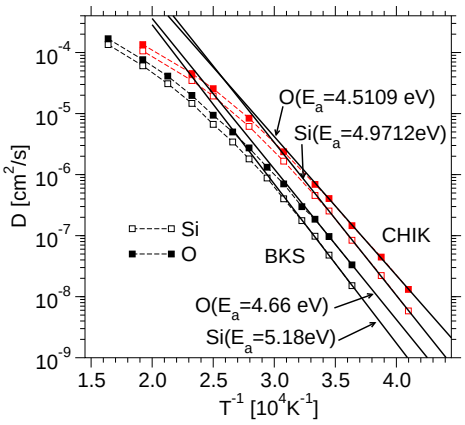

Figure 2. Arrhenius plot of the self-diffusion constants obtained by simulations with the BKS and the CHIK potential, as indicated. The bold solid lines are fits with Arrhenius laws (see text).

found in $g_{\mathrm{SiSi}}(r)$, but also in this case the CHIK potential leads to a better agreement with CPMD than the BKS potential (see the inset in Fig. 1a).

The partial pair correlation functions as obtained from the CPMD runs were used to parameterize the CHIK potential. That these functions are well reproduced by the CHIK potential is thus not that surprising. A less obvious test is provided by considering the distribution functions $P_{\alpha\beta\gamma}(\theta)$ of the bond angles ($\alpha\beta\gamma = \mathrm{OSiO}, \mathrm{SiOSi}$) in comparison to CPMD. As can be inferred from Fig. 1b, the average intra-tetrahedral OSiO angle is around $\theta = 106^\circ$ at 3600 K, both for CPMD and classical MD. However, in the case of the BKS model the function P_{OSiO} is less broad and exhibits a significantly higher amplitude than the CPMD and the CHIK model. Larger differences are seen in the distribution function for the inter-tetrahedral SiOSi angle. While the BKS distribution shows a maximum around $\theta = 147^\circ$, the CHIK model gives a maximum around $\theta = 141^\circ$, in better agreement with the CPMD value around $\theta = 136^\circ$. All the three distribution functions for the SiOSi angle exhibit also a shoulder around $\theta = 90^\circ$ revealing the emergence of edge-sharing tetrahedra at the relatively high temperature $T = 3600\,\mathrm{K}$[15]. In the BKS case, the latter shoulder has a lower amplitude which indicates a smaller number of edge-sharing tetrahedra. Furthermore, as for P_{OSiO} the BKS function for P_{SiOSi} is less broad and its main peak has a higher amplitude. In this sense the BKS model leads to a less disordered structure than the CPMD and the CHIK model.

Detailed comparisons between the CHIK and the BKS model have been also performed with respect to dynamic quantities. Here, we discuss the behaviour of the self-diffusion constants D_α ($\alpha = \mathrm{Si}, \mathrm{O}$). In this case, we take results for the BKS model from a recent simulation study[16]. Whereas the latter results were obtained at the constant density $\rho = 2.37\,\mathrm{g/cm^3}$, the simulation with CHIK potential were done at $\rho = 2.21\,\mathrm{g/cm^3}$ (close to the experimental density of amorphous SiO_2 under ambient conditions which is almost constant over the whole temperature range[17]). The self-diffusion constants were computed from the long-time limit of the mean squared displacements $\langle r_\alpha^2(t)\rangle$ via the Einstein relation $D_\alpha = \lim_{t\to\infty}\langle r_\alpha^2(t)\rangle/6t$[5]. In Fig. 2, the temperature dependence of these transport

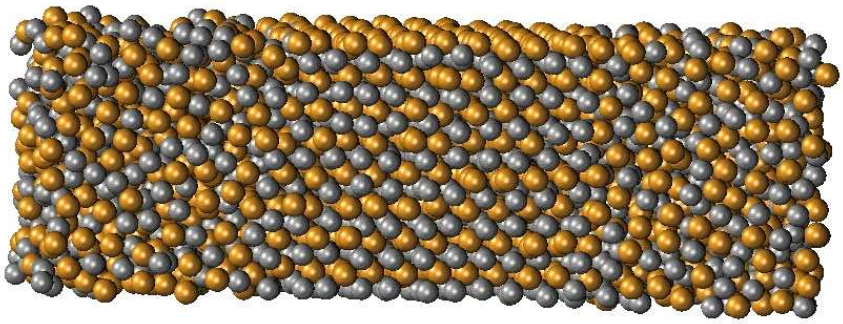

Figure 3. Snapshot of a simulated configuration with two crystal–melt interfaces of the system $Al_{50}Ni_{50}$ at the temperature $T = 1500$ K. Al and Ni atoms are shown as grey and brown spheres, respectively.

coefficients is displayed in an Arrhenius plot. Obviously, the diffusion dynamics, as predicted by the CHIK model, appears to be faster than that of the BKS model. At low temperatures, the self-diffusion coefficients are about a factor of 5 higher than those obtained from the BKS model.

In agreement with various experimental studies[17], at low temperatures the self-diffusion constants can be well-described by an Arrhenius law, $D_\alpha = A_\alpha \exp[-E_\mathrm{a}^\alpha/(k_B T)]$. The activation energies E_a, that we find for the CHIK model, are 4.51 eV for oxygen and 4.97 eV for silicon. These values are very similar to those obtained for the BKS model[16] and they are in good agreement with experimental results ($E_\mathrm{a} = 4.7$ eV for oxygen[18] and $E_\mathrm{a} = 6.0$ eV for silicon[19]). It is remarkable that the temperature dependence of the self-diffusion constants of the CHIK model is very similar to that of the BKS model, although the structure, as obtained from both models, shows significant differences. A dynamic quantity, that is more sensitive to structural differences, is the vibrational density of states. As discussed in Ref.[6], the CHIK model for this quantity yields better agreement with CPMD than the BKS model.

In conclusion, we have developed a new effective potential for silica. The main aim of this work was to develop a fitting scheme for deriving effective (pair) potentials from *ab initio* simulations (CPMD). The new CHIK potential is superior to the BKS model with respect to various static and dynamic properties of amorphous silica. Moreover, as shown in Ref.[6], the CHIK potential has proved to be transferable also to crystalline SiO_2 phases such as α quartz, considering the quantitative agreement between the experimental data for both cell parameters and elastic constants. In the future, our fitting scheme can be used to parameterize potentials for other (amorphous) systems, in particular for mixtures of SiO_2 with other oxides such as Al_2O_3, Na_2O, or MgO.

3 Crystal Growth Kinetics of B2–$Al_{50}Ni_{50}$

To investigate the crystallization of $Al_{50}Ni_{50}$ from the melt, we have done extensive molecular dynamics computer simulations in the NpT ensemble[1–4], i.e., at constant particle number N, constant temperature T and constant pressure ($p_\mathrm{ext} = 0$). The interactions

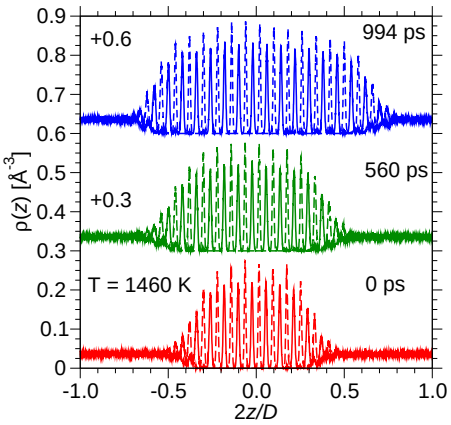

Figure 4. Number density profiles during crystal growth at $T = 1460\,\mathrm{K}$ for Al (dashed lines) and Ni (solid lines). The profiles corresponding to $t = 560\,\mathrm{ps}$ and $t = 994\,\mathrm{ps}$ are shifted with respect to the $t = 0\,\mathrm{ps}$ profiles by 0.3 Å and 0.6 Å, as indicated.

between the atoms were modelled by a potential of the embedded atom (EAM) type, proposed by Mishin *et al.*[20]. Recent studies have shown that this potential gives a realistic description of the diffusion dynamics in Al-Ni melts[21,22] as well as lattice parameters and elastic constants of B2-$Al_{50}Ni_{50}$[20].

At each temperature in the range $1600\,\mathrm{K} \geq T \geq 1200\,\mathrm{K}$, 12 independent samples with solid-liquid interfaces were prepared. To this end, the B2 phase of $Al_{50}Ni_{50}$ was equilibrated at the target temperature for 1 ns. The simulations were done for a system of $N = 3072$ particles ($N_{\mathrm{Al}} = N_{\mathrm{Ni}} = 1536$) in an elongated simulation box of size $L \times L \times D$ (with $D = 3 \times L$), considering the (100) direction of the crystal. Periodic boundary conditions were employed in all three spatial directions. Having relaxed the crystal sample, one third of the particles in the middle of the box were fixed and the rest of the system was melted during 500 ps at $T = 3000\,\mathrm{K}$. Then, the whole system was annealed at the target temperature for another 500 ps, before we started the production runs over 1 ns in the NpT ensemble. A snapshot of the system with two interfaces at $T = 1500\,\mathrm{K}$ is shown in Fig. 3.

The behaviour of samples as the one shown in Fig. 3 depends strongly on the temperature at which they are simulated. While below the melting temperature T_{m}, the crystal will grow, it will melt above T_{m}. From the simulation, the velocity v_{I} with which the liquid-crystal interface moves can be determined. At $T = T_{\mathrm{m}}$, the interface velocity v_{I} vanishes. Thus, by the extrapolation $v_{\mathrm{I}} \to 0$, the melting temperature T_{m} can be estimated. In the following, we show that this procedure yields a rather accurate estimate of T_{m}.

Figure 4 displays the partial number density profiles $\rho(z)$ of Al and Ni at $T = 1460\,\mathrm{K}$ along the z direction, i.e. perpendicular to the solid-liquid interfaces. The lower profiles in Fig. 4 correspond to the starting configuration, while the second and the third ones correspond to $t = 560\,\mathrm{ps}$ and 994 ps. Note that in Fig. 4 the z coordinate is scaled by the factor $2/D$, placing $z = 0$ in the middle of the simulations box. Whereas the crystal structure leads to pronounced peaks in $\rho(z)$, a constant density is observed for the liquid regions

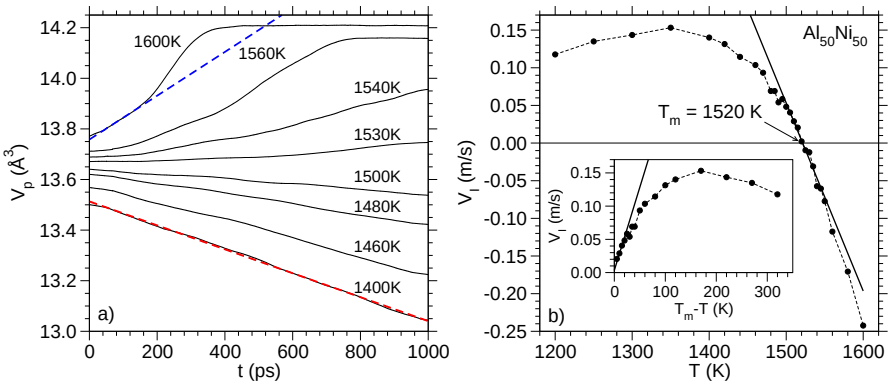

Figure 5. a) Volume per particle, V_p, as a function of time for different temperatures, as indicated. The bold dashed lines are examples of linear fits from which the volume velocity $\dot{V}$ is determined. b) Interface velocity as a function of temperature (filled circles, the dashed line is a guide to the eye). The bold line is a linear fit, $V_\mathrm{I} = k(T_\mathrm{m} - T)$, yielding the kinetic growth coefficient $k = 0.0025\,\mathrm{m/s/K}$ and the melting temperature $T_\mathrm{m} = 1520\,\mathrm{K}$. The inset shows the interface velocity as a function of undercooling $T_\mathrm{m} - T$.

along the z direction, as expected. We can also infer from Fig. 4 that the intermetallic B2 phase (here in (100) orientation) exhibits a pronounced chemical ordering, characterized by the alternate sequence of Al and Ni layers. This indicates that, different from one-component metals, the crystal growth kinetics relies on local rearrangements in the liquid structure. Thus, one may expect that diffusive transport is required to bring the atoms of each species to a suitable site in the B2 crystal. As one can further see in Fig. 4, the crystal is growing at $T = 1460\,\mathrm{K}$. Thus, this temperature is below the melting temperature of our $\mathrm{Al_{50}Ni_{50}}$ model.

Since the density of the crystalline B2 phase is higher than that of the liquid phase, the total volume of the system decreases at temperatures $T < T_\mathrm{m}$ whereas it increases above T_m. Figure 5a shows the time dependence of the volume per particle, V_p, for different temperatures between 1400 K and 1600 K. From this plot, one can infer that the melting temperature is between 1500 K and 1530 K. Also shown in Fig. 5a are examples of linear fits of the form $f(t) = A - \dot{V}_\mathrm{p} t$. Such linear growth laws are expected for steady state growth[23]. We use these fits to determine the change of the volume $\dot{V}$ per unit time. The deviations from the linear behaviour at short times reveal that the growth (or melting) of the crystal is not yet in a steady state regime[23]. At high temperatures, we see a complete melting of the crystal and thus the volume V_p reaches a constant at long times corresponding to the specific volume of the liquid phase. Prior to this, the melting of the crystal is faster than in the linear steady-state regime. In this intermediate regime the crystal has shrunk to such small dimensions that we see essentially the interaction between the two interfaces in the simulation box and thus strong deviations from steady state melting are observed.

From the volume change $\dot{V}_\mathrm{p}$, the velocity v_I, with which the liquid-crystal interfaces move, can be estimated as follows:

$$v_\mathrm{I} = \frac{\dot{V}_\mathrm{p}}{2N_\mathrm{l}(V_\mathrm{c} - V_\mathrm{l})} d \qquad (1)$$

Here, the product $N_\mathrm{l}(V_\mathrm{c} - V_\mathrm{l})$ quantifies the increase of the volume caused by the addition of a crystalline layer (with N_l the average number of particles in a layer, and V_c and V_l the specific volumes of the crystal and the liquid phase, respectively). The length d is the spacing between crystalline layers.

Figure 5b displays the interface velocity v_I as a function of temperature. We see that v_I vanishes around 1520 K and thus this temperature is the estimate for the melting temperature T_m of our simulation model. Note that the experimental value for T_m is around 1920 K and so our simulation underestimates the experimental value by about 20%. Around T_m, the simulation data for v_I can be fitted by the linear law $V_\mathrm{I} = k(T_\mathrm{m} - T)$ where the fit parameter k is the so-called kinetic coefficient. The fit, that is shown in Fig. 5b, yields the value $k = 0.0025$ m/s/K. This value is about two orders of magnitude smaller than the typical values for kinetic coefficients that have been found in simulations of one-component metals[24–27].

The inset in Fig. 5b shows the interface velocity as a function of undercooling $\Delta T = T_\mathrm{m} - T$. We see that v_I increases linearly up to an undercooling of about 30 K. At $\Delta T \approx 180$ K, the interface velocity reaches a maximum value of about 0.15 m/s. Note that our simulation data are in good agreement with recent experimental data on $Al_{50}Ni_{50}$, measured under reduced gravity conditions during a parabolic flight campaign[10].

The very low value of the kinetic coefficient indicates that the crystal growth in $Al_{50}Ni_{50}$ is limited by mass diffusion in the liquid, as proposed by the classical model by Wilson[8] and Frenkel[9]. However, we show in Ref.[11] that, based on sensible assumptions of various parameters, even the Wilson-Frenkel model overestimates the kinetic coefficient for $Al_{50}Ni_{50}$ by at least one order of magnitude. The reason for this can be elucidated by the simulation which reveals that mass diffusion in the liquid-crystal interface controls crystal growth. Since the diffusion in the interface region is much slower than in the bulk liquid, the kinetic coefficient is much lower than expected from the Wilson-Frenkel model.

4 Conclusions

We have presented extensive MD simulation studies that address central issues of materials modelling. The first part was devoted to the development of a new effective potential for silica. We have presented a fitting scheme for deriving effective pair potentials from *ab initio* simulations (CPMD). The method may be used for various molecular systems for which CPMD provides a realistic description. In the second part, the crystallization kinetics of $Al_{50}Ni_{50}$ was investigated. We have shown that the MD simulation gives microscopic insight into the growth kinetics. This is an example that demonstrates the importance of simulation studies, since, at least for metallic alloys, the crystal growth on an atomistic scale is almost not accessible experimentally.

Acknowledgments

A.C. thanks Schott Glas for financial support. The first part of this work is based on collaborative work with Simona Ispas and Walter Kob. For the second part, valuable discussions with Dieter Herlach and Andreas Meyer are gratefully acknowledged. We gratefully

acknowledge financial support within the Priority Program 1120 *Phase Transformations in Multicomponent Melts* of the Deutsche Forschungsgemeinschaft (DFG). Allocation of computer time on the JUMP at the Forschungszentrum Jülich is gratefully acknowledged.

References

1. M.P. Allen and D.J. Tildesley, *Computer Simulation of Liquids* (Clarendon Press, Oxford, 1987).
2. K. Binder and G. Ciccotti (eds.) *Monte Carlo and Molecular Dynamics of Condensed Matter Systems* (Societá Italiana di Fisica, Bologna, 1996).
3. D. Frenkel and B. Smit, *Understanding Molecular Simulation: From Algorithms to Applications* (Academic Press, San Diego, 1996).
4. K. Binder, J. Horbach, W. Kob, W. Paul, and F. Varnik, J. Phys.: Condens. Matter **16**, S429 (2004).
5. K. Binder and W. Kob, *Glassy Materials and Disordered Solids: An Introduction to Their Statistical Mechanics* (World Scientific, London, 2005).
6. A. Carré, J. Horbach, S. Ispas, and W. Kob, submitted to Europhys. Lett. (2007).
7. R. Car and M. Parrinello, Phys. Rev. Lett. **55**, 2471 (1985).
8. H.A. Wilson, Phil. Mag. **50**, 238 (1900).
9. J. Frenkel, Phys. Z. Sow. **1**, 498 (1932).
10. S. Reutzel, H. Hartmann, P.K. Galenko, S. Schneider, and D.M. Herlach, Appl. Phys. Lett. **91**, 041913 (2007).
11. A. Kerrache, J. Horbach, and K. Binder, submitted to Europhys. Lett. (2007).
12. W. Kohn and L. Sham, Phys. Rev. **140**, A1133 (1965).
13. B.W.H. van Beest, G.J. Kramer, and R.A. van Santen, Phys. Rev. Lett. **64**, 1955 (1990).
14. A. Carré, L. Berthier, J. Horbach, S. Ispas and W. Kob, J. Chem. Phys. **127**, 114512 (2007).
15. K. Vollmayr, W. Kob and K. Binder, Phys. Rev. B **54**, 15808 (1996).
16. J. Horbach and W. Kob, Phys. Rev. B **60**, 3169 (1999).
17. O.V. Mazurin, M. V. Streltsina. and T.P. Shvaiko-Shvaikovskaya, *Handbook of Glass Data, Part A: Silica Glass and Binary Silicate Glasses* (Elsevier, Amsterdam, 1983).
18. J.C. Mikkelsen, Appl. Phys. Lett. **45**, 1187 (1984).
19. G. Brébec, R. Seguin, C. Sella, J. Bevenot and J.C. Martin, Acta Metall. **28**, 327 (1980).
20. Y. Mishin, M.J. Mehl and D.A. Papaconstantopoulos, Phys. Rev. B **65**, 224114 (2002).
21. S.K. Das, J. Horbach, M.M. Koza., S. Mavila Chathoth and A. Meyer, Appl. Phys. Lett. **86**, 011918 (2005).
22. J. Horbach, S.K. Das, A. Griesche, M.-P. Macht, G. Frohberg and A. Meyer, Phys. Rev. B **75**, 174304 (2007).
23. H.E.A. Huitema, M.J. Vlot and J.P. van der Eerden, J. Chem. Phys. **111**, 4714 (1999).
24. J.J. Hoyt and M. Asta, Phys. Rev. B **65**, 214106 (2002).
25. D.Y. Sun., M. Asta and J.J. Hoyt, Phys. Rev. B **69**, 024108 (2004).
26. Z.G. Xia, D.Y. Sun, M. Asta and J.J. Hoyt, Phys. Rev. B **75**, 012103 (2007).
27. K.A. Jackson, Interface Sc. **10**, 159 (2002).